Origami-Like 3-D Folded MEMS Approach for Miniature Inertial Measurement Unit

Alexandra Efimovskaya, *Student Member, IEEE*, Yu-Wei Lin, *Student Member, IEEE*, and Andrei M. Shkel, *Fellow, IEEE*

***Abstract*— This paper presents a miniature 50 mm^3 inertial measurement unit (IMU) implemented using a folded micro-electromechanical systems (MEMS) process. The approach is based on wafer-level fabrication of high aspect-ratio single-axis sensors interconnected by flexible hinges and folded into a 3-D configuration, like a silicon Origami [1]. Two different materials for flexible hinges have been explored, including photo-definable polyimide and parylene-C. We report, for the first time, an IMU prototype with seven operational sensors: three accelerometers, three gyroscopes, and a prototype of a reference clock. This paper concludes with the results of experimental characterization of inertial sensors demonstrating the feasibility of the proposed approach for a compact IMU. [2016-0267]**

***Index Terms*— 3-D microelectromechanical systems (MEMS), inertial measurement unit, inertial sensors, micro-assembly.**

I. Introduction

MEMS-BASED Inertial Measurement Units (IMUs) provide an advantage of small size, low power, and low cost, which resulted in their fast adoption in consumer electronics, such as mobile phones and gaming devices. A scope of applications of consumer IMUs includes activity detection, virtual and augmented reality, optical and electronic image stabilization, to name a few. Over the last years, there has been a continuous improvement in performance of MEMS consumer inertial sensors. Present day ultra-compact consumer IMUs can be used for tracing position and orientation for a short duration of time (on the order of few seconds), but not yet applicable for self-contained navigation (from minutes to hours of navigation). Due to fast accumulating errors, they are used in a combination with magnetometers, altimeters and other sensors, as a short-term backup system, when GPS or other location sources are temporarily lost or interrupted.

Meanwhile, a number of high performance silicon MEMS sensors have been recently reported in literature, for example a degenerate mode Disk Resonator Gyroscope, [2], or a Quadruple Mass Gyroscope, [3]. Noise characteristics of these devices showed a potential for achieving the navigation grade accuracy. A technology enabling an efficient way to assemble the high-end inertial sensors into a 6-axis IMU configuration, while preserving advantages of a relatively compact size and low cost, may enable a wide range of demanding applications. Some potential applications include uninterrupted personal navigation in presence of jamming/spoofing of RF signals and navigation of small, fast, highly maneuverable unmanned vehicles in GPS-challenged environments, [4].

Most conventional methods to implement a compact MEMS IMU fall into two general categories. The first method is based on discrete assembly of 6 individual sensors, [5]– [8]. Using this approach, off-the-shelf single-axis sensors are assembled manually into a 3D IMU configuration. Single-axis sensors are typically optimized to reject off-axis inputs, allowing for improved IMU performance. However, this approach generally results in increased size and weight of the IMU, since it requires an assembly of 6 separate Printed Circuit Boards (PCB), each carrying a single sensor. For example, utilizing the discrete assembly approach, a tactical grade IMU has been demonstrated by Honeywell [5] and a near-tactical grade IMU by Sensonor [8].

Another method, a so-called single-chip approach, is based on fabrication of multi-axes or single-axis sensors on a single chip. Utilizing a single chip approach, very small volume (<10 mm^3) consumer IMUs have been reported, such as a miniature multi-axis IMU in 10.9 mm^3 volume by Fairchild [9], a compact six degrees-of-freedom inertial sensor by Analog Devices [10], iNEMO inertial module in 6.5 mm^3 volume by ST Micro [11], and a 6-axis Motion Tracking device in 8.1 mm^3 volume by InvenSense [12]. Single-chip approach delivers an advantage of extremely small volume, often at the cost of sub-optimal performance. For example, in multi-axis-sensor implementation, where a single mechanical element is used for measuring rotation and/or acceleration in multiple directions, a cross-talk between axes of sensitivity is a potential challenge. In the case of a single-chip implementation of multiple single-axis devices, the in-plane and out-of-plane sensors are fabricated on the same substrate or placed alongside. In such implementation, different devices generally pursue self-contradicting objectives, and a compromise in performance must be ultimately made. For example, implemented alongside of the Z axis sensor, the X- and Y-axis gyroscopes with the out-of-plane detection mode often suffer from large quadrature errors, [13]. In addition, high signal-to-noise ratio sensors, like degenerate mode gyroscopes in [2] and [14], are typically designed only

Manuscript received November 3, 2016; revised February 28, 2017; accepted April 13, 2017. Date of publication June 13, 2017; date of current version September 29, 2017. This work was supported in part by the Defense Advanced Research Projects Agency and in part by U.S. Navy under Contract N66001-13-1-4021. Subject Editor H. Seidel. *(Corresponding author: Alexandra Efimovskaya.)*

The authors are with the Microsystems Laboratory, University of California at Irvine, Irvine, CA 92697 USA (e-mail: aefimovs@uci.edu; yuweil4@uci.edu; andrei.shkel@uci.edu).

Color versions of one or more of the figures in this paper are available online at http://ieeexplore.ieee.org.

Digital Object Identifier 10.1109/JMEMS.2017.2703594

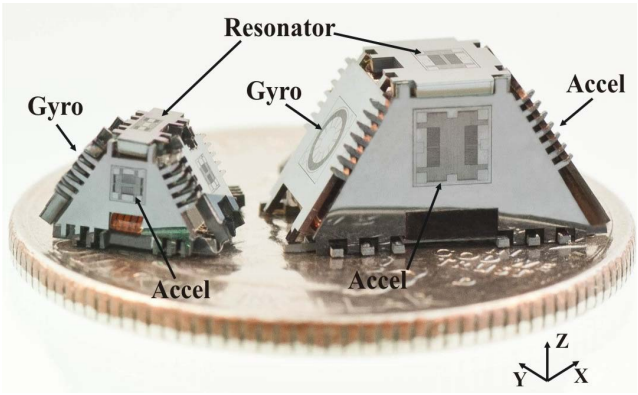

Fig. 1. Fabricated IMU prototypes in 15 mm^3 and 50 mm^3 volume (for size comparison, on a coin of quarter of US dollar). When folded in a 3-D configuration, devices allow for 3-DOF orientation, 3-DOF positioning, and timing data.

for in-plane operation (for measuring rotation around Z axis). Due to lack of symmetry in XZ and YZ planes of SOI devices, a single-chip implementation of such sensors for all three axes of sensitivity is challenging.

In this paper, we explore an alternative fabrication paradigm for implementation of potentially a high-performance miniature IMU, Fig.1. Folded MEMS process is based on a wafer-level fabrication of flat structures with single-axis high aspect-ratio SOI (Silicon-on-Insulator) sensors, which are optimized for a single-axis measurement. Flexible polymer hinges connecting the sensors array enable folding a flat microsystem into a 3D IMU configuration, like a silicon origami, [1]. Combining advantages of conventional MEMS fabrication processes, folded IMU technique permits a significant reduction in size, as compared to the discrete assembly approach, without compromises in device performance, [15].

Using flexible polymer hinges to achieve vertical and 3D structures with conventional silicon bulk and surface micromachining has been previously reported in literature. Suzuki *et al.* [16], demonstrated rigid poly-Si plates connected by elastic polyimide hinges to mimic the flapping motion of a butterfly wing for microrobotic applications. Polyimide hinges have been utilized for vertical parallel-plate microactuators, created by folding silicon plates [17]. Zara *et al.* [18], explored the use of polyimide as a mechanical material for micro-mirror hinges. Ataka and Fujita [19] demonstrated a concept of the "smart MEMS sheet" composed of a micro actuator array on a flexible polyimide film, compatible with any arbitrary curved 3D shape.

Along with polyimide, parylene is another emerging polymeric material for fabrication of 3D foldable structures. Several research groups demonstrated metal coils folded into 3D shapes using parylene flexible hinges [20]–[21]. Ding *et al.* [22], proposed a process with hydrogel-parylene bilayer to fabricate self-folding 3D micro-structures. Parylene is widely used for biomedical devices, for example in fabrication of 3D flexible micro-probes for neural signal recording applications, [23], [24], and 3D spherical origami structures with electrodes for intra-ocular implantation, [25].

Folded MEMS approach for implementation of a multi-axis IMU was first demonstrated by the research group at UC Irvine, [26]. The method utilized a 3D foldable SOI structure with in-situ fabricated inertial sensors. A planar structure was fabricated and subsequently folded in a pyramidal shape, forming a compact IMU. The inter-locking latches located along the edges of each sidewall of a pyramid were used to lock the panels in a 3D structure. The sidewalls were then fused together to maintain the alignment of sensors and improve the IMU structural rigidity. In the single-sided fabrication process, high-aspect ratio sensors and polyimide hinges were fabricated on the front side of the SOI wafer. Electrical interconnects were formed on the same side of the wafer and served to transmit signals from the sidewall to the base of the structure. In this approach, metal interconnects enabled the interface between sensors and external signal conditioning electronics.

Along with all the advantages of the single-sided Folded IMU approach [26], including a relatively simple 4-mask fabrication process, a small size of IMU, structural rigidity, and compatibility with the wafer-level packaging process, several challenges emerged during the initial studies. First, the thick layer of polyimide on the device side of a wafer limited the accuracy of lithography resulting in reduced performance of inertial sensors. Second, placing the sensors and the metal traces on the same side of the wafer introduced challenges associated with cleaning of devices at the end of the fabrication. This significantly decreased the yield of the overall process, and fabrication runs did not result in fully operational IMUs. Additionally, the electrical connections between the front and the handle side of the wafer were not available as a part of the process. As a result, in the previously reported approach, the inner volume of the folded structure could not be used, for example, for integration with signal processing electronics.

In this work, we report the most recent developments in Folded 3D MEMS technology, introducing an alternative double-sided process for fabrication of high-performance miniature IMU. In the following sections, we will first introduce the double-sided Folded IMU concept, Section II. We will then present the fabrication sequence and discuss the choice of material for flexible hinges, Section III. In Section IV, we will present the design of the inertial sensors integrated on the Folded IMU sidewalls. This will be followed by experimental characterization of the fabricated prototypes, Section V, demonstrating feasibility of the approach. Section VI concludes the paper with a discussion of results.

II. Double-Sided Folded IMU Concept

Folded MEMS IMU approach is based on a double-sided Silicon-on-Insulator (SOI) process for fabrication of flat foldable MEMS structures, on a wafer-level. In our process, both sides of the SOI wafer are efficiently utilized. Inertial sensors are created on the device side of the wafer (Fig. 2a), while metal interconnects and polymer flexible hinges are formed on the handle side of the wafer (Fig. 2b).

The front and the handle side of the SOI wafer are electrically connected using thru-wafer copper interconnects. The technology of Thru-Wafer Interconnects for Double-Sided (TWIDS) realization of sensors on SOI wafers is an

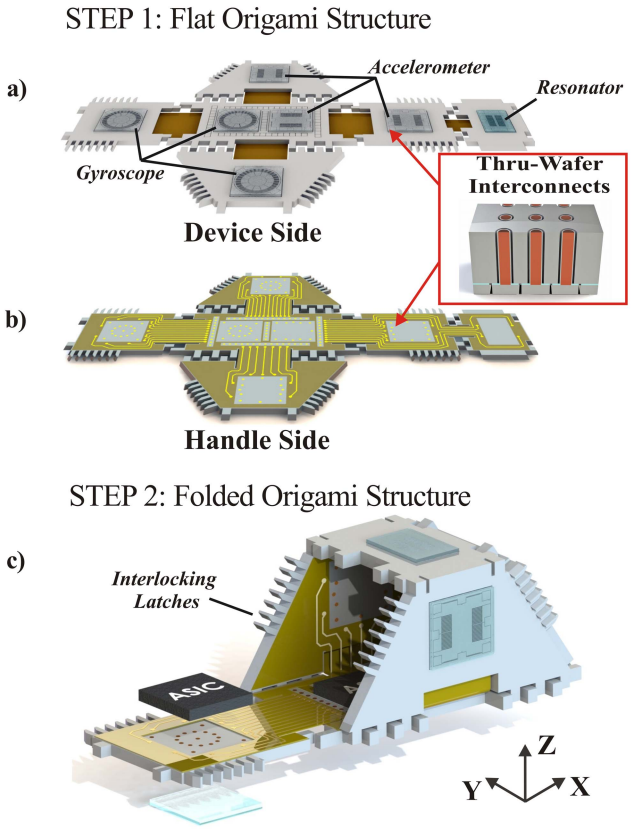

Fig. 2. Folded MEMS IMU: (a) device side of a flat structure, (b) handle side of a flat structure, (c) folded structure. Double-sided fabrication process and thru-wafer interconnects enable efficient utilization of the IMU inner volume.

integral part of the Folded IMU process, [28]. Based on bottom-up seedless copper electroplating, TWIDS approach enables high aspect-ratio ultra-low resistance vertical electrical connections.

Thru-wafer interconnects provide a path for electrical signals from sensors on the device side of the wafer to the handle side of the wafer. This facilitates IMU integration with electronic components integrated inside the 3D structure. Such efficient utilization of the inner volume results in reduction of the finial product dimensions.

Every IMU device is comprised of at least three single-axis gyroscopes and three single-axis accelerometers. In addition, a clock might be co-integrated with IMU to provide timing information along with position and orientation, or as a reference clock for signal processing. All sensors are designed to have a single axis of sensitivity and are optimized to reject off-axis inputs. We take advantage of a thick device layer of the SOI wafer for improved sensitivity of high aspect-ratio inertial sensors and increased immunity to vibration perpendicular to substrate. Flexible hinges enable folding of a flat device into a 3D configuration.

Devices are usually implemented on the front side of the folded structure to provide an easy access for inspection and probing. Alternatively, to protect the sensors from environment, Folded IMU can be implemented with sensors on the inner faces of the silicon panels and metal traces on the outer faces. Placing the sensors inside the 3D structure is possible due to the thru-wafer via and does not result in any changes of the fabrication process flow. However, when placing flexible hinges on the outside, the hinge length has to be increased to account for substrate thickness and allow for folding.

Once folded, IMU allows for measurement of 3-DOF orientation, 3-DOF positioning, and timing data (Fig. 2c). The change in alignment of sensors' axes of sensitivity during operation is the factor contributing to degradation of IMU performance. To maintain the original alignment of sensors (after the calibration) under different environmental conditions, the Folded IMU structures are reinforced by means of epoxy, eutectic soldering, or silicon welding of the interlocking latches located along the silicon panels. It was previously shown in [26] that solder reinforced IMU structures exhibit <0.2 mrad change in sidewall alignment angle during thermal testing in the range of temperatures from 25°C to 85°C. The misalignment error due to temperature can be further minimized using silicon welding for reinforcement of IMU structures, [27].

III. Fabrication

A. Process Flow

The manufacturing process for double-sided folded TIMU starts with Deep Reactive Ion Etching (DRIE) of 500 μm deep blind via holes patterned on the handle-side of the SOI wafer, Fig. 3a. This is followed by removal of 5 μm buried oxide layer inside the via holes to permit an electrical contact with the 100 μm device layer. The via holes are then filled with copper using sonic-assisted seedless electroplating method. This approach does not require any additional conductive seed layer deposition, but utilizes a highly doped silicon device layer as a seed for electroplating, Fig. 3b. The technique assures void-free features and allows for high density array of ultra-low resistance thru-wafer interconnects, [29]. The aspect ratio of the interconnects varies for different sensor designs and is usually in the range from 6:1 to 10:1 (wafer thickness to copper stem diameter), [28].

Following the fabrication of interconnects, the polymer flexible hinges are defined on the handle-side of the wafer. Metal traces are then created on top of the polymer insulating layer, Fig. 3c. Next, the donut-shape insulating gaps are etched around the copper filled vias, completing the handle-side processing, Fig. 3d.

Top-side processing starts with creating a SiO_2 hard mask, Fig. 3e. This is followed by etching of sensor features and thru-wafer etch, which is necessary for separation of panels for subsequent folding in a 3-D shape, Fig. 3f. The thru-wafer etch is performed by, first, covering the sensors with a layer of photoresist, then DRIE etching of a 100 μm device layer, removing buried oxide, and DRIE etching of a 400 μm handle wafer, Fig. 3e. At this point, the thru-wafer etch is not complete and another 100 μm of the handle wafer needs to be removed. This is done by stripping off the photoresist protective layer to open the sensors features and continuing the etching, using the previously defined SiO_2 hard mask. During this fabrication step, the sensors and the last 100 μm of the handle wafer are etched in parallel, Fig. 3f. The sensors are then released, using vapor HF.

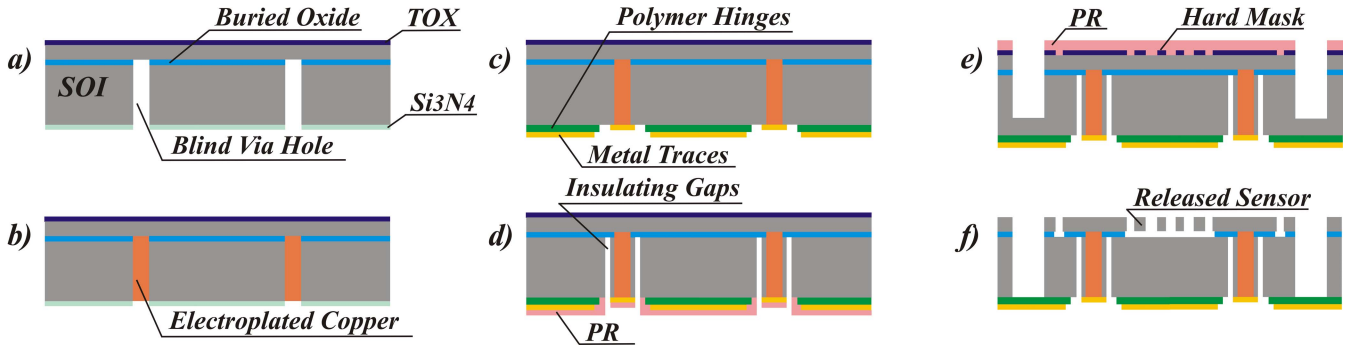

Fig. 3. 6-Mask wafer-level fabrication process for double-sided IMU with thru-wafer interconnects: a) Deep Reactive-Ion Etching (DRIE) of blind via holes, b) filling the via holes with copper using seedless electroplating method, c) formation of polymer flexible hinges and metal traces on the handle-side of the wafer, d) DRIE of insulating gaps, e) sensors hard mask definition and top-side pre-etch, f) top-side thru-wafer etch and sensors release.

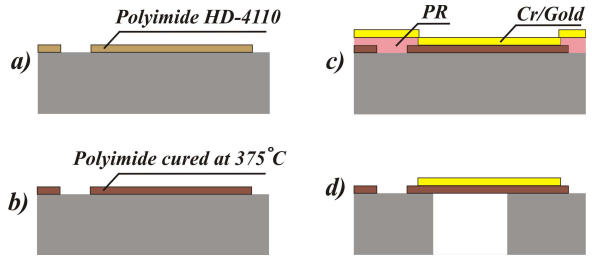

Fig. 4. Fabrication of polyimide flexible hinges: a) polyimide deposition using spin-coating of substrate, b) curing to enable extensive polymer cross-linking, c) metal traces formation using lift-off process, d) silicon back-side etching.

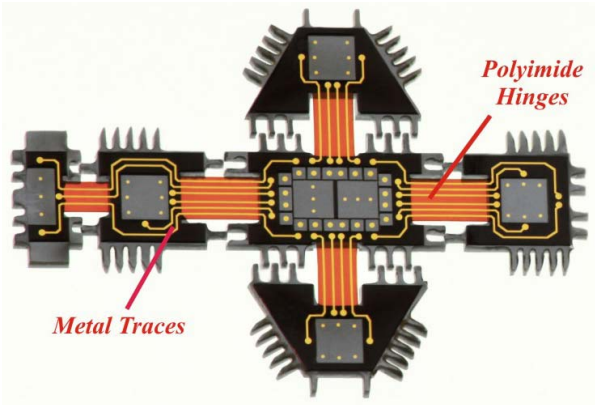

Fig. 5. Micro-photograph of a fabricated foldable IMU structure with 15 μm thick polyimide flexible hinges and metal traces.

B. Flexible Hinges

Formation of flexible polymer hinges is a critical step in the "Origami" MEMS process. Hinges allow for folding of flat microstructures to form a three-dimensional IMU device. In addition to the mechanical support of the device panels, the polymer material provides the electrical insulation for the network of metal traces. Therefore, while choosing the material for flexible-hinge fabrication, both electrical and mechanical properties need to be considered.

Photodefinable polyimide is widely used for fabrication of flexible structures. It has garnered much attention as a structural material due to its many favorable features, including low YoungâŁ™s modulus (3.4 GPa) and excellent electrical properties, such as a low dielectric constant, high volume, and surface resistivity. Polyimide is typically spin-coated and cured at high temperature. Once cured, the polyimide film is resistant to most solvents and chemicals.

The process flow for polyimide flexible-hinge fabrication is shown in Fig. 4. The HD-4110 polyimide is first deposited on the substrate by spin-coating, then the pattern is photo-lithographically defined, Fig. 4a. To improve the adhesion of polyimide to the silicon nitride surface the VM-652 adhesion promoter is used, available from HD MicroSystems. The thickness of polyimide layer before curing is 28 μm. Once the polyimide is deposited and patterned, it is cured at 375°C in the nitrogen environment, Fig. 4b. One hour of curing enables extensive polymer cross-linking, which provides mechanical and chemical robustness. After polyimide is fully cured, the final film thickness is approximately 15 μm. Following the polyimide deposition, a 0.05 μm thick Cr adhesion layer and a 0.5 μm gold layer are evaporated, Fig. 4c. Lift-off process is utilized to pattern the metal and define the electrical traces and the contact pads features, Fig. 4d.

Parylene-C is another polymer which has recently gained interest as a structural material for fabrication of 3D foldable structures, and it was also explored in this work. Parylene is a polymer deposited using vapor deposition at a room temperature; it is chemically inert and stable, while having a very high surface and volume resistivity and low Youngs modulus (2-5 GPa). With an elongation-to-break percentage of more than 200%, parylene-C is a preferable material for applications requiring large deflections. In addition, parylene is virtually not out-gassing, which is critical for vacuum packaging of IMU devices.

The process flow for fabrication of parylene flexible hinges starts with E-Beam deposition of 50 nm Cr layer, which enables an improved adhesion between the parylene layer and a Si wafer, Fig. 6a. An alternative option to use Silane A-174 as an adhesion promoter was also explored. However, this material was concluded to be not compatible with a subsequent HF release step. Adhesion promoter, Silane A-174, is damaged during prolonged immersion in HF solution, resulting in a loss of adhesion of the parylene film and easy peeling off.

TABLE I
MECHANICAL, ELECTRICAL, AND THERMAL PROPERTIES OF POLYIMIDE AND PARYLENE C

	Polyimide	Parylene C
Tensile Strength (MPa)	200	96
Elongation to Break (%)	45	200
Dielectric Constant @ 1kHz	3.2	3.1
Volume Resistivity (Ohm-cm)	$3.3x10^{16}$	$8.8x10^{16}$
Maximum Temperature (°C)	350	290

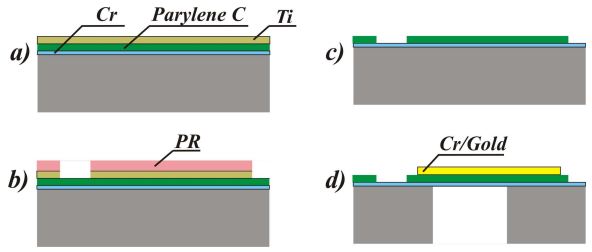

Fig. 6. Fabrication of parylene flexible hinges: a) Cr adhesion layer and parylene deposition, followed by Ti layer evaporation, b) Ti mask etching, c) parylene etching using RIE, d) metal traces formation and silicon back-side etching.

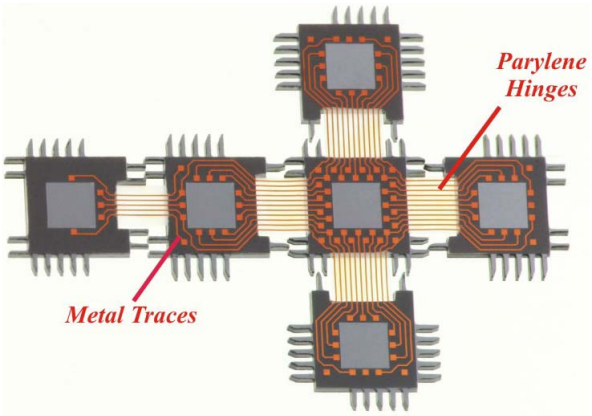

Fig. 7. Micro-photograph of a foldable IMU structure with 16 μm thick parylene-C flexible hinges and metal traces.

A vacuum deposition system (SCS Labcoter 2) is used to deposit a 16 μm thick film of parylene-C. This is followed by evaporation of a 150 nm thick Ti layer, which serves as a mask for parylene etching. The AZ nLOF 2035 photoresist lithography is performed to define the flexible hinges and the Ti mask is etched using Reactive Ion Etching (RIE), Fig. 6b. Next, we RIE process the parylene and etch the photoresist layers, Fig. 6c. This part of the process completes with immersing the wafer into a 20 % hydrofluoric acid (HF) solution for 1 min to remove the Ti residue redeposited onto the wafer during the RIE etching. Metal traces on top of the parylene are created using E-Beam evaporation of Cr adhesion layer (0.05 μm) and gold layer (0.5 μm), followed by the lithography step and metal lift-off, Fig. 6d.

The critical mechanical, electrical and thermal properties of polyimide and parylene C are summarized in Table I. In order to compare advantages of different polymers for flexible hinges, foldable IMU structures with HD-4110 polyimide and with parylene-C hinges were fabricated, Fig.5 and Fig.7.

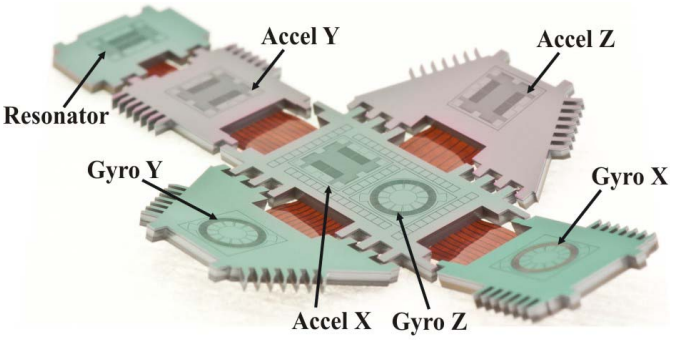

Fig. 8. "Origami-like" Folded MEMS TIMU (Timing and Inertial Measurement Unit) with in-situ fabricated three gyroscopes, three accelerometers and a resonator (prototype of a reference clock).

Using polyimide has an advantage of a simple deposition process, where a wafer is spin-coated with a thick polymer film. Polyimide, however, requires curing. It has been noticed that after the heat treatment at high temperatures (>350°C) the polyimide film does not allow for easy plastic deformation and is less suitable for folding. Bending of polyimide hinges from 0 to 120° resulted in forming cracks in the film. For larger plastic deformation, a lower curing temperature has to be considered [16], but the adjustment might potentially lead to degradation in the mechanical, chemical, and dielectric properties of the film. In contrast to polyimide, parylene is deposited using a vacuum vapor deposition process, which requires up to 6 hours for a 16 μm thick film. Parylene, however, does not require curing. Fabricated IMU prototypes with parylene hinges showed superior quality of the film after folding: no cracking or traces delamination were observed.

Both polymers were experimentally demonstrated to survive the prolonged temperature treatment at 285°C for Parylene C and at 350°C for polyimide HD-4110. This opens a path for wafer-level vacuum packaging and chip-level ceramic packaging of Folded IMU.

However, due to the described advantageous properties of parylene, it was selected as a material for flexible hinges in the most recent folded IMU fabrication runs.

IV. SENSORS DESIGN

Folded 3D MEMS process allows for parallel fabrication of foldable structures and different types of SOI-based inertial sensors. IMU prototypes, featuring three single-axis accelerometers, a resonator (prototype of a reference clock), and three single-axis gyroscopes, is shown in Fig.8. Performance of the stand-alone inertial sensors was demonstrated in our previous publications, [14]–[32]. The sensors were modified for compatibility with the Folded MEMS process. In this work, we report the devices integrated on sidewalls of the foldable IMU structures.

The static open-loop single-axis SOI accelerometer has a footprint of 3×3 mm and is comprised of a suspended proof-mass, Fig. 9(a). Accelerometers were designed to operate at the resonant frequency of 650 Hz. Two pairs of differential electrodes with parallel plates are used for sensing the capacitance change under the applied acceleration.

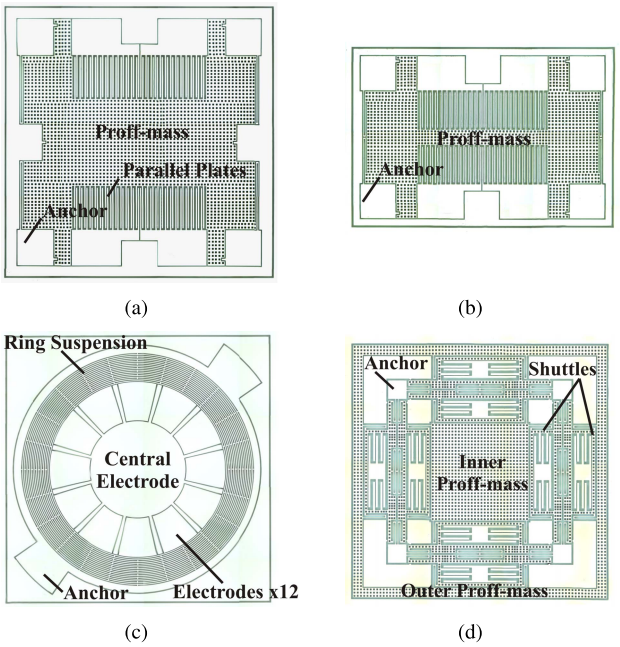

Fig. 9. IMU prototypes are comprised of three single-axis accelerometers, a resonator (prototype of a reference clock), and three single-axis gyroscopes. (a) Accelerometer architecture. (b) Resonator architecture. (c) 2.8 mm diameter Toroidal Ring. Gyroscope (TRG) (d) 3.1 mm Dual Foucault Pendulum (DFP) gyroscope.

For technology demonstration, a nominal gap of 7 μm between the parallel plates was chosen. However, for the double-sided fabrication process presented in this paper, the minimum gap is limited only by the silicon etching aspect ratio. Since the state-of-the-art DRIE aspect ratios are usually between 50:1 and 100:1 [30], the minimum gap in Folded IMU process can be potentially reduced to <2 μm.

Similar to the accelerometer, a resonator is comprised of the suspended proof-mass, Fig. 9(b). The sensor footprint is 2×3 mm. It is designed to operate at 5.6 kHz frequency. The resonator is included as a prototype of the master clock, which can serve all frequency-reference functions in IMU.

For the purpose of performance comparison, two types of single-axis SOI gyroscopes are implemented on the sidewalls of the Folded IMU test structures: Toroidal Ring Gyroscope (TRG) [14] and Dual Foucault Pendulum (DFP) [32]. However, only one of the designs is sufficient for the IMU implementation. The designs of these gyroscopes were previously introduced in our publications. In order to enable integration with the Folded IMU, the sensors dimensions and several critical features were modified as described below.

The Toroidal Ring Gyroscope (TRG), first implemented in the epitaxial silicon encapsulation (EpiSeal) process, was initially introduced in [14]. It is comprised of an inner electrode assembly, an outer support, and a ring suspension, Fig. 9(c). The inner electrode assembly consists of 12 radial electrodes that are used as a forcer and as a pick-off for each of the wineglass modes. Design adaptation for the Folded MEMS IMU process resulted in increased diameter (from 1.76 to 2.8 mm), increased capacitive gap (from 1.5 to 7 μm), and reduced operational frequency (from 60 kHz to 14 kHz). The suspension system was formed by the sixteen 10 μm thick concentric rings. The gyroscope was designed to operate in the n=3 wineglass modes, which are the lowest in frequency ordering among all modes of the structure, [31]. Since the diameter of the TRG can be further reduced to approximately 1.4 mm, this design is most suitable for ultra-miniature IMUs with a volume of less than 15 mm^3.

The dynamically balanced Dual Foucault Pendulum (DFP) gyroscope, fabricated using an SOI MEMS process, was first introduced in [32]. The central element of the sensor is two mechanically coupled and dynamically equivalent proof-masses (inner mass and outer mass), oscillating in anti-phase motion, Fig. 9(d). Dynamic balance is achieved by using identical (mirrored) suspension elements and shuttle assemblies as well as by aligning the center of masses of each proof-mass. The center of mass of the system remains stationary during oscillation, causing the net force and torques generated by the combined system to be zero at all times. Electrostatic transduction of the sensor is realized using the arrays of parallel plates located within the shuttle assemblies. The design is most suitable for a medium-size IMUs. Each sidewall of a 50 mm^3 volume Folded IMU has a 3.16×3.16 mm opening for a sensor. To enable integration on the sidewalls of a Folded IMU device, the footprint of the original DFP design is reduced from 6.7 to 3.1 mm. In order to compensate for a significant reduction in sensor capacitance, the nominal gap was reduced from 8 to 6 μm, resulting in 2.7 pF total capacitance. The sensor was designed to operate in anti-phase mode at 8 kHz resonant frequency.

V. Experimental Results

The double-sided Folded IMU fabrication run, with in-situ fabricated sensors and metal traces on polyimide, resulted in $>80\%$ yield of operational sensors and yielded 10 out of 15 fully operational IMU devices (with all 7 sensors operational in the IMU).

Folded IMU prototypes were die-attached to an adapter board, packaged into a 181-pin, gold plated through-hole Ceramic Pin Grid Array (CPGA) package, and assembled with front-end electronics. IMU prototypes in 50 mm^3 volume with all seven sensors operational were demonstrated, thus confirming feasibility of the proposed fabrication approach, Table II.

Wafer-level vacuum packaging of Folded IMU as well as the IMU-level ceramic packaging using SST vacuum packaging tool (SST International) are currently under development. All accelerometers presented in this paper were tested in air, and all gyroscopes were tested in a vacuum chamber at 0.5 mTorr vacuum.

Frequency domain characterization showed the resonant frequency of the resonator at 5.57 kHz and the resonant frequencies of 3 accelerometers spaced at 640, 648 and 670 Hz. Characterization of Toroidal Ring Gyroscopes co-fabricated on the IMU sidewalls revealed frequency splits of 10 Hz, 35 Hz and 220 Hz at the center frequencies of 14 kHz, 15 kHz, and 15.9 kHz, correspondingly, with a Q-factor of 100,000 at 0.5 mTorr vacuum. Frequencies of devices are separated by design in order to minimize cross-talk between sensors.

TABLE II

EXPERIMENTAL FREQ. RESPONSE CHARACTERIZATION OF THE INERTIAL SENSORS IN-SITU FABRICATED ON THE SIDEWALLS OF THE SAME FOLDED TIMU DEVICE

Sensor	Type	Frequency, f_c	Freq. Split, Δf
Accel X	Accelerometer	648 Hz	-
Accel Y	Accelerometer	640 Hz	-
Accel Z	Accelerometer	670 Hz	-
Resonator	Resonator	5.57 kHz	-
Gyro X	Toroidal Ring Gyroscope (TRG)	14 kHz	10 Hz
Gyro Y	Toroidal Ring Gyroscope (TRG)	15 kHz	35 Hz
Gyro Z	Toroidal Ring Gyroscope (TRG)	16 kHz	220 Hz

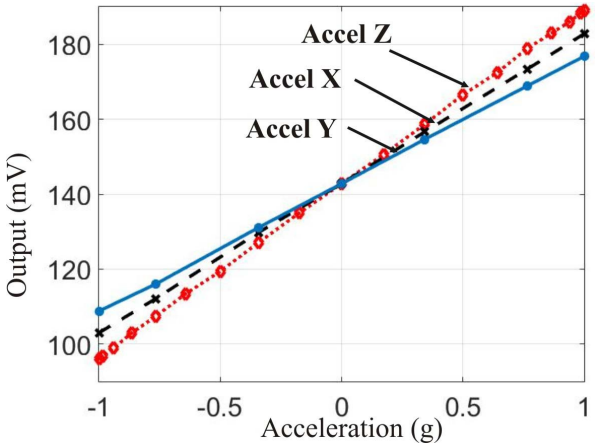

Fig. 10. Tilt-table characterization revealed SF of 39.9, 46.2, and 34 mV/g for X, Y, and Z accelerometers integrated on the sidewalls of a Folded TIMU prototype.

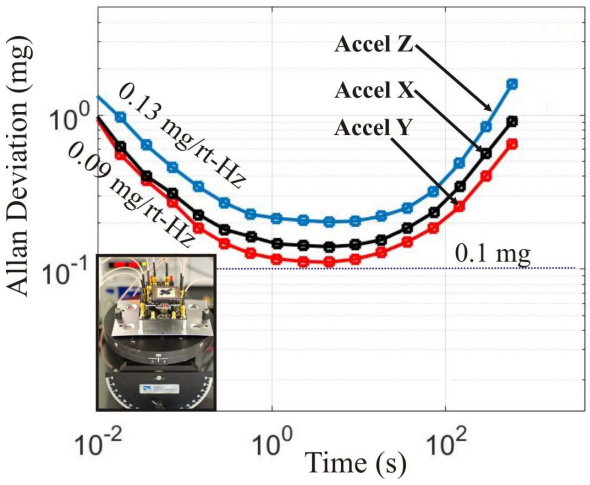

Fig. 11. (a) TRG response to the rate-table sinusoidal input with amplitude of 5 deg and frequency of 1 Hz, (b) DFP response to the rate-table sinusoidal input with amplitude of 10 deg and frequency of 1 Hz.

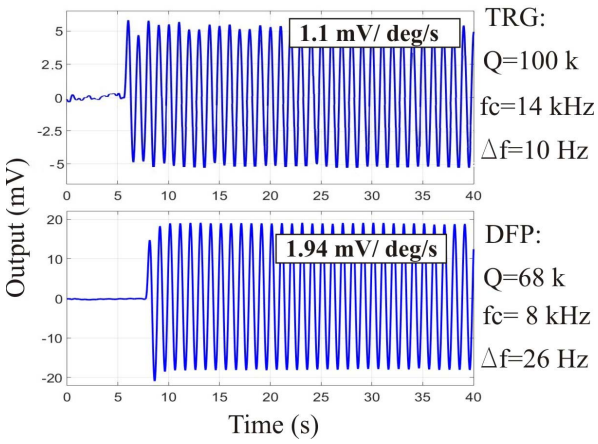

Fig. 12. Noise analysis of the X, Y, and Z accelerometers on the TIMU sidewalls revealed bias stability of 0.1 mg and velocity random walk (VRW) of 0.09 $mg/\sqrt{Hz}$.

In order to derive the accelerometerâŁ™s scale factor, the IMU prototype and the signal processing electronics were mounted on the tilt table. The accelerometer response test was conducted by tilting the stage 90 deg around the X and Y axes, providing ± 1 g of acceleration amplitude. The carrier demodulation with a Zurich Instruments lock-in amplifier was used to measure the output current. A low-noise fully input/output differential amplifier (Texas Instrument Op. Amp. THS4131) was used in a transimpedance configuration in order to convert current to voltage, as well as to increase the signal-to-noise ratio. The scale factors of 39.9, 46.2, and 34 mV/g were measured for X, Y, and Z accelerometers, correspondingly, Fig. 10. Experimental characterization of three accelerometers showed in-run bias instability as low as 0.1 mg and VWR of 0.09 $mg/\sqrt{Hz}$, Fig. 11.

Performance of the accelerometers was limited by noise of the signal processing electronics. Analytically calculated thermal mechanical noise of the accelerometer is lower than 0.35 $\mu g/\sqrt{Hz}$. Electronics optimization may allow for improved performance.

Dynamic response of the gyroscopes was tested using the capability of Ideal Aerosmith 2102 Series Two-Axis Position and Rate Table System, allowing to produce a rotation with programmed sinusoidal angular acceleration. Electrostatic actuation and capacitive detection were employed for gyroscopes operation. The gyroscopes were excited with a constant DC voltage and an AC voltage generated by a Phase Locked Loop. A carrier signal at frequency of 100 kHz was applied to the proof-mass, resulting in the amplitude modulation of the sensor output. The output signal was then demodulated to reveal the low frequency changes in capacitance. The amplitude of the drive-mode motion was stabilized, using an Automatic Gain Control (AGC), [34].

All loops were realized using a Zurich Instruments HF2LI digital lock-in amplifier. Initial characterization of TRG was performed in an open loop configuration without mode-matching of the devices. DFP frequency split was tuned down to <3 Hz, using electrostatic tuning with 28.5 V tuning voltage applied to the y-axis forcer electrodes. Lower DC bias voltages can be used if y mode pick-off electrodes are used for electrostatic tuning, in addition to the forcer electrodes. Rate table experiment revealed the TRG scale factor of 1.1 mV/(deg/s)

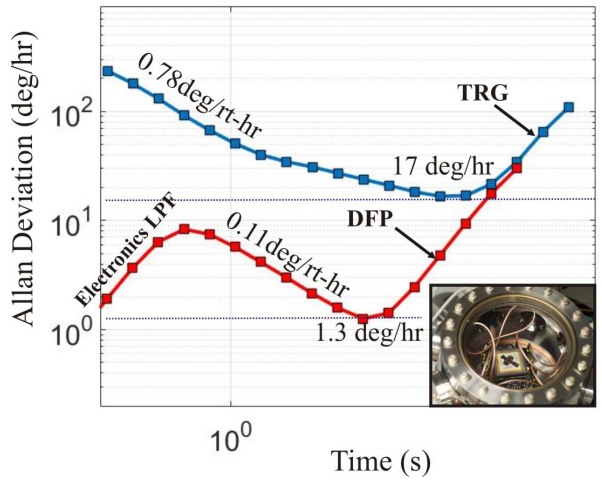

Fig. 13. Noise analysis of the TRG revealed bias stability of <17 deg/h and ARW of 0.78 $deg/\sqrt{h}$; noise analysis of the DFP revealed bias stability of <1.3 deg/h and ARW of 0.11 $deg/\sqrt{h}$.

TABLE III
EXPERIMENTALLY TESTED PARAMETERS OF THE ACCELEROMETERS ON THE IMU SIDEWALLS

	Accel X	**Accel Y**	**Accel Z**
Scale Factor, mV/g	39.9	34.0	46.2
Velocity Random Walk, $mg/\sqrt{Hz}$	0.09	0.09	0.13
Bias Instability, mg	0.14	0.1	0.2

TABLE IV
EXPERIMENTALLY TESTED PARAMETERS OF THE GYROSCOPES ON THE IMU SIDEWALLS

	TRG	**DFP**
Scale Factor, $mV/(deg/s)$	1.1	1.94
Angle Random Walk, $deg/\sqrt{h}$	0.78	0.11
Bias Instability, deg/h	17	1.3
Quadrature Error, deg/s	237	404

and the DFP scale factor of 1.94 mV/(deg/s), Fig.12. The Root Allan Variance Analysis (r-AVAR) was used for identification of random noise characteristics. Experimental characterization of the TRG showed bias stability of <17 deg/h and ARW of 0.78 $deg/\sqrt{h}$; experimental noise analysis of the DFP showed bias stability of <1.3 deg/h and ARW of 0.11 $deg/\sqrt{h}$, Fig. 13.

Measured performance parameters of the sensors implemented on the IMU sidewalls are summarized in Tables III and IV. For tactical grade IMU, a quadrature error of the gyroscopes, arising from coupling between the drive and the sense modes, has to be considered. This error contributes to the gyroscope performance resulting in bias shifts [33]. For the TRG, the quadrature error of 237 deg/s without electromechanical compensation was measured before folding the device. During this test, a flat IMU device was attached to the ceramic package using a temporary attachment with an indium alloy. The device was then folded and the quadrature error of 227 deg/s was measured. This result suggested that the stresses during folding do not cause significant change in quadrature error.

VI. CONCLUSION

We have presented a Folded MEMS approach for fabrication of miniature IMUs. The approach is based on folding an array of single-axis inertial sensors into a 3D IMU configuration, using polymer flexible hinges. This technique permits a significant reduction in IMU size while preserving the sensor performance. We introduced a new double-sided process for fabrication of flat foldable MEMS IMU structures on a wafer-level. In our process, inertial sensors are created on the device side of the wafer. In parallel, metal interconnects and polymer flexible hinges are formed on the handle side of the wafer. The double-sided process resulted in increased yield of the Folded IMU fabrication runs. In addition, due to introduction of TWIDS, the inner volume of the folded structure can be efficiently utilized for integration with signal processing electronics.

We studied different materials for implementation of flexible hinges, such as photo-definable polyimide and parylene-C. Despite simplicity of the fabrication steps for polyimide hinges, parylene-C was eventually selected as a preferable material for flexible hinges due to a superior quality of the film after folding.

IMU inertial sensors characterization proved feasibility of the Folded MEMS approach for compact tactical grade performance IMU. Characterization of accelerometers showed VRW of 0.09 $mg/\sqrt{Hz}$ and in-run bias instability of <0.1 mg. Noise analysis of the 2.8 mm TRG revealed bias stability of <17 deg/h and ARW of 0.78 $deg/\sqrt{h}$; noise analysis of the 3.1 mm DFP revealed bias stability of <1.3 deg/h and ARW of 0.11 $deg/\sqrt{h}$.

For a tactical-grade IMU, temperature variations is an important factor to consider since temperature-induced long-term bias and scale-factor drifts may limit the IMU performance. One possible source of instability vs temperature is the change in Si panels alignment due to temperature. As we discussed in Section II, IMU structural reinforcement allows for significant reduction of the sidewall misalignment angle under thermal loading. After the IMU panels are enforced by silicon welding, the next remaining most important sources of instability vs temperature in Folded IMU are the temperature sensitivity of the sensors resonant frequencies and frequency mismatch between the vibratory modes, as well as the temperature sensitivity of the Q-factor. In order to improve the long-term stability, different thermal compensation techniques can be potentially implemented. For example, the compensation method utilizing the resonant frequency as a measure of the sensor temperature, [35], or compensation technique utilizing a micro-oven co-fabricated with IMU sensors, [36]. However, these studies are outside the scope of this paper.

Folded IMU presented in this paper is the first demonstration of the double-sided fabrication process. Device miniaturization by means of the shape optimization and reduction of the area occupied by a network of metal traces is possible. In addition, thru-wafer vias would enable placing a part of the signal processing electronics inside the 3D structure, which may result in further reduction in volume. The integration of IMU with electronics is not discussed in this paper.

Folded MEMS IMU can be potentially instrumented in stabilization, guidance and navigation applications, where extremely small size, low weigh and high performance are essential, such as in small unmanned vehicles, missiles, robotics, and personal navigation. Capable of producing 3D MEMS structures, using standard bulk and surface micro-machining tools, Folded MEMS process may serve as a technological platform for applications beyond inertial navigation.

ACKNOWLEDGMENT

Devices were designed, developed, and tested in MicroSystems Laboratory, UC Irvine. The authors would like to thank UCI INRF staff Jake Hes and Mo Kebaili for their help and valuable suggestions on the fabrication aspects of the project. The authors would also like to acknowledge Sina Askari for his help in PCB design and fabrication.

REFERENCES

[1] A. Efimovskaya, D. Senkal, S. Askari, and A. M. Shkel, "Origami-like folded MEMS for realization of TIMU: Fabrication technology and initial demonstration," in *Proc. IEEE Int. Symp. Inertial Sens. Syst.*, Hapuna Beach, HI, USA, Mar. 2015, pp. 1–4.

[2] A. D. Challoner, H. H. Ge, and J. Y. Liu, "Boeing disc resonator gyroscope," in *Proc. IEEE/ION Position Location Navigat. Symp. (PLANS)*, Monterey, CA, USA, May 2014, pp. 504–514.

[3] P. I. Prikhodko, A. A. Trusov, and M. A. Shkel, "North-finding with 0.004 radian precision using a silicon MEMS quadruple mass gyroscope with q-factor of 1 million," in *Proc. IEEE MEMS Conf.*, Paris, France, Jan./Feb. 2012, pp. 164–167.

[4] Y. Mulgaonkar, A. Makineni, K. Mohta, C. J. Taylor, and V. Kumar, "Fast autonomous flight with micro unmanned vehicles," in *Proc. Solid-State Sens., Actuators, Microsyst. Workshop*, Hilton Head Island, SC, USA, Jun. 2016, pp. 28–31.

[5] Honeywell. (2012). *HG1930 IMU*. [Online]. Available: https://www.honeywell.com

[6] Systron Donner. (2014). *SDI500 Tactical Grade IMU*. [Online]. Available: https://www.systron.com

[7] Northrop Grumman. (2013). *MEMS IMU*. [Online]. Available: https://www.northropgrumman.litef.com

[8] Sensonor. (2014). *STIM300 IMU*. [Online]. Available: https://www.sensonor.com

[9] Fairchild. (2015). *FIS1100 MEMS Inertial Measurement Unit*. [Online]. Available: https://www.fairchildsemi.com

[10] Analog Devices. (2014). *ADIS16445 Compact, Precision Six Degrees of Freedom Inertial Sensor*. [Online]. Available: www.analog.com

[11] ST Micro. (2016). *LSM6DSM iNEMO Inertial Module*. [Online]. Available: https://www.st.com

[12] Invensense. (2014). *MPU-6500 Motion Tracking Device*. [Online]. Available: https://www.invensense.com

[13] S. Dellea, F. Giacci, A. Longoni, P. Rey, A. Berthelot, and G. Langfelder, "Large full scale, linearity and cross-axis rejection in low-power 3-axis gyroscopes based on nanoscale piezoresistors," in *Proc. IEEE MEMS*, Estoril, Portugal, Jan. 2015, pp. 37–40.

[14] D. Senkal *et al.*, "100K Q-factor toroidal ring gyroscope implemented in wafer-level epitaxial silicon encapsulation process," in *Proc. IEEE MEMS*, San Francisco, CA, USA, Jan. 2014, pp. 24–27.

[15] A. Efimovskaya, D. Senkal, and A. M. Shkel, "Miniature origami-like folded MEMS TIMU," in *Proc. 18th Int. Conf. Solid-State Sens., Actuators, Microsyst. (Transducers)*, Anchorage, AK, USA, Jun. 2015, pp. 584–587.

[16] K. Suzuki, I. Shimoyama, and H. Miura, "Insect-model based microrobot with elastic hinges," *IEEE J. Microelectromech. Syst.*, vol. 3, no. 1, pp. 4–9, Mar. 1994.

[17] M. Gel and I. Shimoyama, "Parallel-plate electrostatic actuation with vertical hinges," *J. Micromech. Microeng*, vol. 11, no. 5, pp. 555–560, 2001.

[18] J. M. Zara, S. Yazdanfar, K. D. Rao, J. A. Izatt, and S. W. Smith, "Electrostatic micromachine scanning mirror for optical coherence tomography," *Opt. Lett.*, vol. 28, no. 8, pp. 628–630, Apr. 2003.

[19] M. Ataka and H. Fujita, "Micro actuator array on a flexible sheet—Smart MEMS sheet," in *Proc. IEEE MEMS*, Taipei, Taiwan, Jan. 2013, pp. 536–539.

[20] F. Herrault, S. Yorish, T. Crittenden, and M. G. Allen, "Microfabricated, ultra-dense, three-dimensional metal coils," in *Proc. 15th Int. Solid-State Sens., Actuators, Microsyst. Conf. (Transducers)*, Denver, CO, USA, Jun. 2009, pp. 1718–1721.

[21] Y. Zheng, X. Sun, X. Li, and H. Zhang, "Flexible Parylene-based folded inductors with magnetic core," in *Proc. 17th Int. Solid-State Sens., Actuators, Microsyst. Conf. (Transducers)*, Barcelona, Spain, Jun. 2013, pp. 2261–2264.

[22] Z. Ding, P. Wei, and B. Ziaie, "Self-folding smart 3D microstructures using a hydrogel-Parylene bilayer," in *Proc. 18th Biennial Univ./Govt./Ind. Micro/Nano Symp. (UGIM)*, vol. 1. West Lafayette, IN, USA, Jun./Jul. 2010, pp. 1–4.

[23] C. H. Chen *et al.*, "A three-dimensional flexible microprobe array for neural recording assembled through electrostatic actuation," *RSC J. Lab Chip*, vol. 11, no. 9, pp. 1647–1655, 2011.

[24] J. Kuo *et al.*, "3D Parylene sheath probes for reliable, long-term neuroprosthetic recordings," in *Proc. IEEE MEMS*, Taipei, Taiwan, Jan. 2013, pp. 1073–1076.

[25] Y. Liu *et al.*, "Parylene origami structure for intraocular implantation," in *Proc. 17th Int. Solid-State Sens., Actuators, Microsyst. Conf. (Transducers)*, Barcelona, Spain, Jun. 2013, pp. 1549–1552.

[26] S. A. Zotov, M. C. Rivers, A. A. Trusov, and A. M. Shkel, "Folded MEMS pyramid inertial measurement unit," *IEEE Sensors J.*, vol. 11, no. 11, pp. 2780–2789, Nov. 2011.

[27] M. C. Rivers, "Folded MEMS 3-D structures for inertial measurement applications," Ph.D. dissertations, Dept. Mech. Aerosp. Eng., Univ. California, Irvine, CA, USA, 2015.

[28] A. Efimovskaya, Y. Lin, and A. M. Shkel, "Thru-Wafer Interconnects for Double-Sided (TWIDS) fabrication of MEMS," in *Proc. IEEE Inertial Sens. Conf. (Inertial)*, Laguna Beach, CA, USA, Feb. 2016, pp. 66–69.

[29] A. Efimovskaya and A. M. Shkel, "160 milli-ohm electrical resistance thru-wafer interconnects with 10: 1 Aspect ratio," in *Proc. IMAPS Conf.*, San Diego, CA, USA, Oct. 2014, pp. 000505–000510.

[30] K. J. Owen, B. VanDerElzen, R. L. Peterson, and K. Najafi, "High aspect ratio deep silicon etching," in *Proc. IEEE MEMS*, Paris, France, Jan./Feb. 2012, pp. 251–254.

[31] A. Efimovskaya, D. Wang, Y. Lin, and A. M. Shkel, "On ordering of fundamental wineglass modes in toroidal ring gyroscope," in *Proc. IEEE SENSORS*, Orlando, FL, USA, Oct./Nov. 2016, pp. 1–3.

[32] D. Senkal, A. Efimovskaya, and A. M. Shkel, "Dual foucault pendulum gyroscope," in *Proc. 18th Int. Solid-State Sens., Actuators, Microsyst. Conf. (Transducers)*, Anchorage, AK, USA, Jun. 2015, pp. 1219–1222.

[33] M. S. Weinberg and A. Kourepenis, "Error sources in in-plane silicon tuning-fork MEMS gyroscopes," *J. Microelectromech. Syst.*, vol. 15, no. 3, pp. 479–491, Jun. 2006.

[34] I. P. Prikhodko, S. A. Zotov, A. A. Trusov, and A. M. Shkel, "What is MEMS gyrocompassing? Comparative analysis of maytagging and carouseling," *J. Microelectromech. Syst.*, vol. 22, no. 6, pp. 1257–1266, Dec. 2013.

[35] I. P. Prikhodko, A. Alexander Trusov, and M. A. Shkel, "Achieving long-term bias stability in high-Q inertial MEMS by temperature self-sensing with a 0.5 millicelcius precision," in *Proc. Solid-State Sens., Actuators, Microsyst. Workshop*, Hilton Head Island, SC, USA, Jun. 2012, pp. 287–290.

[36] C. H. Ahn *et al.*, "On-chip ovenization of encapsulated disk resonator gyroscope (DRG)," in *Proc. 18th Int. Solid-State Sens., Actuators, Microsyst. Conf. (Transducers)*, Anchorage, AK, USA, Jun. 2015, pp. 39–42.

Alexandra Efimovskaya received the diploma degree (Hons.) in engineering specializing in navigation systems from the Saint-Petersburg State University of Aerospace Instrumentation, Saint-Petersburg, Russia, in 2009, and the M.S. degree in mechanical and aerospace engineering from the University of California at Irvine, Irvine, CA, USA, in 2015, where she is currently pursuing the Ph.D. degree in mechanical engineering with the MicroSystems Laboratory, with a focus on micro-electro-mechanical inertial sensors and systems. The main area of her research is related to design and control of inertial sensors for navigation applications. She was a 2011 Fulbright Scholar and a recipient of the 2015 Amelia Earhart Award for women in an aerospace-related science. She received the Outstanding Paper Award (oral presentation category) at the 18th International Conference on Solid-State Sensors, Actuators, and Microsystems (Transducers'2015), and the Best Student Paper Award (lecture track) at the IEEE/ASME International Symposium on Inertial Sensors (Inertial'2017).

Yu-Wei Lin received the B.S. degree in engineering mechanics from the University of Illinois at Urbana–Champaign, IL, USA, in 2014, and the M.S. degree in mechanical engineering from the University of California at Irvine, Irvine, CA, USA, in 2016, where he is currently pursuing the Ph.D. degree in mechanical engineering. His research interests include design, fabrication, and control of vibratory inertial sensors.

Andrei M. Shkel (F'99) received the diploma degree (Hons.) in mechanics and mathematics from Moscow State University, Moscow, Russia, in 1991, and the Ph.D. degree in mechanical engineering from the University of Wisconsin, Madison, WI, USA, in 1997. In 2000, he joined the Faculty at the University of California at Irvine, Irvine, CA, USA, where he is currently a Professor with the Department of Mechanical and Aerospace Engineering, with a joint appointment in the Department of Electrical Engineering and Computer Science, and the Department of Biomedical Engineering. He served as the Program Manager of the Microsystems Technology Office, Defense Advanced Research Projects Agency (DARPA), Arlington, VA, USA, from 2009 to 2013. His professional interests, reflected in over 200 publications, include solid-state sensors and actuators, microelectromechanical systems-based neuroprosthetics, sensor-based intelligence, and control theory. He holds over 30 U.S. and worldwide patents. His current interests center on the design, manufacturing, and advanced control of high-precision micromachined gyroscopes. He was a recipient of the 2002 George E. Brown, Jr. Award, the 2005 NSF CAREER Award, the 2006 UCI HSSoE Best Faculty Research Award, and the 2009 IEEE Sensors Council Technical Achievement Award. He received the Office of the Secretary of Defense Medal for Exceptional Public Service for his work at DARPA as the Program Manager in 2013. He has served on a number of editorial boards, most recently, as an Editor of the IEEE/ASME JOURNAL OF MICROELECTROMECHANICAL SYSTEMS, and the Founding Chair of the IEEE International Symposium on Inertial Sensors and Systems. He was voted the 2018 President-Elect of the IEEE Sensors Council.